

Torsional rigidity of an elliptic bar with multiple elliptic inclusions using a null-field integral approach

Jeng-Tzong Chen · Ying-Te Lee · Jia-Wei Lee

Received: 13 August 2009 / Accepted: 14 March 2010
© Springer-Verlag 2010

Abstract Following the success of using the null-field integral approach to determine the torsional rigidity of a circular bar with circular inhomogeneities (Chen and Lee in *Comput Mech* 44(2):221–232, 2009), an extension work to an elliptic bar containing elliptic inhomogeneities is done in this paper. For fully utilizing the elliptic geometry, the fundamental solutions are expanded into the degenerate form by using the elliptic coordinates. The boundary densities are also expanded by using the Fourier series. It is found that a Jacobian term may exist in the degenerate kernel, boundary density or boundary contour integral and cancel out to each other. Null-field points can be exactly collocated on the real boundary free of facing the principal values using the bump contour approach. After matching the boundary condition, a linear algebraic system is constructed to determine the unknown coefficients. An example of an elliptic bar with two inhomogeneities under the torsion is given to demonstrate the validity of the present approach after comparing with available results.

Keywords Torsional rigidity · Null-field integral equation · Degenerate kernel · Elliptic coordinates · Jacobian

1 Introduction

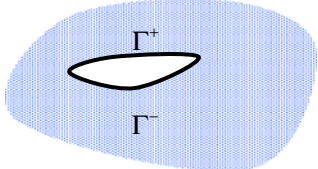
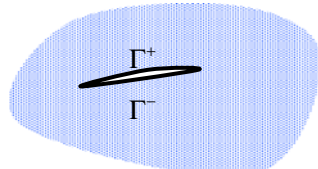
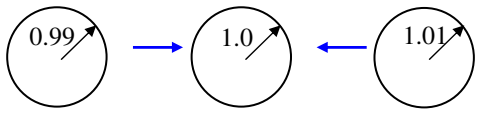
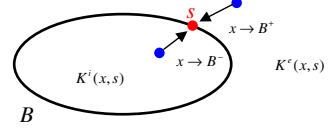
For solving boundary value problems (BVPs) of elasticity, it is always difficult to find an analytical solution which satisfies the partial differential equations and given boundary conditions at the same time except for some simple cases. In the elasticity textbooks [1–3], there are many simple and classical problems, e.g. a torsion problem of an elliptic bar. An exact or analytical solution is very useful as a benchmark example for engineers and researchers while they develop a new numerical approach. For a special case, the semi-inverse solution may be found a priori such that it satisfies the governing equation and boundary condition. We can obtain the exact solution through this way only for a lucky case, but it is not a logical way. For example, the Saint-Venant torsion solution [1–3] of an elliptic bar is a typical case which was obtained by using the semi-inverse method. To derive the analytical solution in a rational manner, Zhong and co-workers [4] presented a new approach based on the Hamiltonian principle and the symplectic duality system. Here, we focus on the approach of boundary integral equation method (BIEM) to derive the semi-analytical solution in a logical manner.

For a complex problem of an elliptic bar with multiple holes or inclusions, the analytical solution is not easy to be obtained by using the semi-inverse method. Therefore, the numerical approaches are usually resorted. Katsikadelis and Sapountzakis [5] used the boundary element method to solve torsion problems of an elliptic bar with two elliptic inclusions. Not only torsional rigidity but also shear stress was obtained. Chou and Shamas-Ahmadi [6] extended the complex variable boundary element method (CVBEM) developed by Hromadka and Lai [7] to solve torsion problems of hollow shafts. In their case of an elliptic bar with two symmetrical elliptic holes, the discrepancy is found between their

J.-T. Chen (✉) · Y.-T. Lee · J.-W. Lee
Department of Harbor and River Engineering, National Taiwan Ocean University, Keelung 20224, Taiwan
e-mail: jtchen@mail.ntou.edu.tw

J.-T. Chen
Department of Mechanical and Mechatronic Engineering, National Taiwan Ocean University, Keelung 20224, Taiwan

Table 1 Degenerate cases in mathematics and mechanics

Terminology	General situation	Degenerate case
Degenerate eigenvalue	Various eigenvalues ($\lambda_1 \neq \lambda_2$)	Two eigenvalues merge together ($\lambda_1 \rightarrow \lambda_2$).
Degenerate boundary	Two different boundaries 	Two boundaries coincide together ($\Gamma^+ \rightarrow \Gamma^-$). 
Degenerate scale	Scale a_n (normal)	Two normal scales approach a degenerate scale (critical scale, $a_n \rightarrow a_c$). 
Degenerate kernel	Separable form $K(x, s) = \begin{cases} K^i(x, s) = \sum_{k=1}^n p_k(x)q_k(s), & x \leq s , \\ K^e(x, s) = \sum_{k=1}^n p_k(s)q_k(x), & x > s . \end{cases}$	Two expressions (interior and exterior) merge together when $x \rightarrow B^+$ and B^- . 
	Galerkin method (Double integrals) $\int_B \int_B K(x, s) dB(s) dB(x)$	Double integrals merge to single integral. $\int_B p(s) dB(s) \int_B q(s) dB(s)$

results and those of Katsikadelis and Sapountzakis [5]. Later, they also used the CVBEM to deal with problems of composite shafts [8]. The data are better than the previous results [6]. Sapountzakis and Mokos [9–11] also used the boundary element method to solve torsion problems. They concerned on nonuniform torsion of composite bars. However, it is not a pure boundary element method (BEM) in their formulation since their method needed the domain discretization in the axis of the bar to evaluate integrals.

Recently, Chen et al. [12–22] applied the null-field boundary integral method in conjunction with the degenerate kernel and Fourier series to solve many problems with circular boundaries. Basic and classical problems, e.g. two classical elasticity problems, Lamé problem and the problem of stress concentration factor, were also revisited by using the approach [17]. Also, torsion problems containing circular holes and/or inclusions [13, 19] have been solved. They claimed that this approach is a semi-analytical approach since error attributes from the truncation of number of terms of Fourier series. Furthermore, it can obtain the closed-form solution for the simple cases, e.g. circular and annular cases. Nevertheless, all of their examples were focused on circular boundaries. Therefore, we will extend this idea to deal with torsion problems with elliptic holes and/or inclusions in this paper.

The term of “degenerate” often occurs for the special case that two representations merge to one, e.g. degenerate

boundary, degenerate scale and degenerate eigenvalue as shown in Table 1. In the Fredholm integral equations, the degenerate kernel plays an important role. However, its applications in practical problems seem to have taken a back seat to other methods. This method can be seen as one kind of approximation methods, and the kernel function is expressed as finite sums of products by two linearly independent functions as follows:

$$K(x, s) = \sum_{k=1}^n p_k(x)q_k(s).$$

Sometimes, the degenerate kernel is called separable kernel since the source and field points are separated. This terminology is not coined by the authors, but follows the literature [23–25]. The concept of generating “optimal” degenerate kernels has been proposed by Sloan et al. [26]. They also proved it to be equivalent to the iterated Petrov-Galerkin approximation. Later, Kress [27, 28] proved that the integral equations of the second kind in conjunction with degenerate kernels have the convergence rate of exponential order instead of the linear algebraic order. The convergence rate is better than that of the conventional BEM. In the literature, it is observed that exact solutions for boundary value problems are only limited for simple cases. Therefore, proposing a semi-analytical approach for solving boundary value

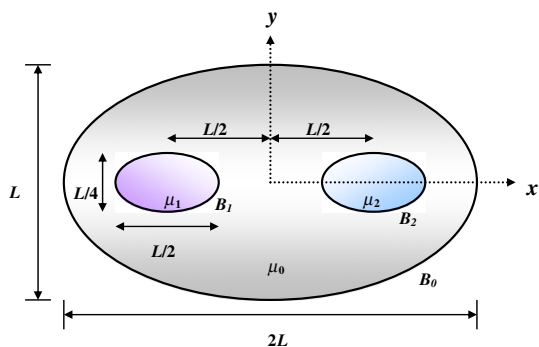


Fig. 1 A composite elliptic bar

problems with elliptic boundaries of arbitrary numbers, various size and different positions is our goal here.

In this paper, we employ a systematic approach to deal with Saint-Venant torsion problem of an elliptic bar with elliptic inclusions. A null-field integral formulation is utilized in conjunction with the degenerate kernel and the Fourier series. To fully utilize the elliptic geometry, the fundamental solution is expanded to the degenerate kernel by using the elliptic coordinates which were provided in the Morse and Feshback’s book [29]. Also, the boundary densities are expanded by using the Fourier series in conjunction with a Jacobian term. The advantage of free of calculating principal value by using the bump contour is gained even though the null-field point is exactly located on the real boundary. Not only stress but also torsional rigidity can be obtained by using the present method. Finally, an example with two elliptic inhomogeneities is used to verify the validity of the present approach after comparing with the numerical results in the literature.

2 Problem statement

An elliptic bar containing two elliptic inclusions bounded to the contours $B_k (k = 0, 1, 2)$ is shown in Fig. 1. We define

$$B = \bigcup_{k=0}^2 B_k. \tag{1}$$

The semiaxes of elliptic bar and inclusions are also shown in Fig. 1. The elliptic bar twisted by couples applied at the end is taken into consideration. Following the theory of Saint-Venant torsion [3], the warping function φ must satisfy the Laplace equation,

$$\frac{\partial^2 \varphi}{\partial x^2} + \frac{\partial^2 \varphi}{\partial y^2} = 0 \quad \text{in } D, \tag{2}$$

where D is the domain. Since the traction-free condition is specified on the outer boundary, we have

$$\frac{\partial \varphi}{\partial n} = 0 \quad \text{on } B_0. \tag{3}$$

The continuity condition for the displacement and equilibrium condition for traction on the interface between the matrix and inclusion are

$$\varphi_i^M = \varphi_i^I \quad \text{on } B_i, \tag{4}$$

$$\mu_0 \frac{\partial \varphi_i^M}{\partial n} - \mu_i \frac{\partial \varphi_i^I}{\partial n} = (\mu_0 - \mu_i)(yn_x - xn_y) \quad \text{on } B_i, \tag{5}$$

where the superscripts “I” and “M” denote the inclusion and matrix, respectively, μ_0 is the shear modulus for the matrix and μ_i is the shear modulus for the i th inclusion.

3 Method of solution

3.1 Dual null-field integral formulation

By introducing the degenerate kernels, the collocation point can be located on the real boundary free of facing singularity. Therefore, the representations of conventional integral equations including the boundary point can be written as

$$2\pi \varphi(x) = \int_B T(s, x)\varphi(s) dB(s) - \int_B U(s, x)\psi(s) dB(s), \tag{6}$$

$$x \in D \cup B,$$

$$2\pi \frac{\partial \varphi(x)}{\partial n_x} = \int_B M(s, x)\varphi(s) dB(s) - \int_B L(s, x)\psi(s) dB(s), \tag{7}$$

$$x \in D \cup B,$$

and

$$0 = \int_B T(s, x)\varphi(s) dB(s) - \int_B U(s, x)\psi(s) dB(s), \tag{8}$$

$$x \in D^c \cup B,$$

$$0 = \int_B M(s, x)\varphi(s) dB(s) - \int_B L(s, x)\psi(s) dB(s), \tag{9}$$

$$x \in D^c \cup B,$$

where s and x are the source and field points, respectively, $\psi(s) = \frac{\partial \varphi(s)}{\partial n_s}$, n_s and n_x denote the unit outward normal vectors at the source point s and field point x , respectively, and the kernel function $U(s, x) = \ln r$, ($r \equiv |s - x|$), is the fundamental solution which satisfies

$$\nabla^2 U(s, x) = 2\pi \delta(x - s), \tag{10}$$

in which $\delta(x - s)$ denotes the Dirac-delta function. The other kernel functions, $T(s, x)$, $L(s, x)$, and $M(s, x)$, are defined by

$$T(s, x) = \frac{\partial U(s, x)}{\partial n_s}, \tag{11}$$

$$L(s, x) = \frac{\partial U(s, x)}{\partial n_x}, \tag{12}$$

$$M(s, x) = \frac{\partial^2 U(s, x)}{\partial n_s \partial n_x}, \tag{13}$$

once the kernel is expressed in term of an appropriate degenerate form. It is noted that x in Eqs. (6)–(9) can exactly locate on the real boundary. The detail information can be found in [19].

3.2 Expansions of fundamental solution and boundary density

Based on the null-field integral formulation as previously mentioned, it is noted that the key point of the present method is the use of the degenerate kernel. To fully use the elliptic geometry, we expand the fundamental solution into a degenerate form by using the property of an elliptic coordinates. It is well known that the closed-form fundamental solution of the Laplace problem is

$$U(s, x) = \ln r. \tag{14}$$

Based on the separable property, $U(s, x)$ can be expanded into degenerate form by separating the source points and field points in the elliptic coordinates [29] as given below:

$$U(s, x) = \begin{cases} U^i(\bar{\xi}, \bar{\eta}; \xi, \eta) = \bar{\xi} + \ln \frac{c}{2} \\ \quad - \sum_{m=1}^{\infty} \frac{2}{m} e^{-m\bar{\xi}} \cosh m\xi \cos m\eta \cos m\bar{\eta} \\ \quad - \sum_{m=1}^{\infty} \frac{2}{m} e^{-m\bar{\xi}} \sinh m\xi \sin m\eta \sin m\bar{\eta}, & \bar{\xi} \geq \xi, \\ U^e(\bar{\xi}, \bar{\eta}; \xi, \eta) = \xi + \ln \frac{c}{2} \\ \quad - \sum_{m=1}^{\infty} \frac{2}{m} e^{-m\xi} \cosh m\bar{\xi} \cos m\eta \cos m\bar{\eta} \\ \quad - \sum_{m=1}^{\infty} \frac{2}{m} e^{-m\xi} \sinh m\bar{\xi} \sin m\eta \sin m\bar{\eta}, & \bar{\xi} < \xi, \end{cases} \tag{15}$$

where (ξ, η) is the elliptic coordinates, $s = (\bar{\xi}, \bar{\eta})$, $x = (\xi, \eta)$, the superscripts “ i ” and “ e ” denote the interior ($\xi \leq \bar{\xi}$) and exterior ($\xi > \bar{\xi}$) cases, respectively. It is worthy of noting that the larger argument is contained in the leading term and denominator. It is also found that the form in Eq. (15) is similar to the degenerate kernel of the polar coordinate system. But it has a rigid body term ($\ln \frac{c}{2}$) when the elliptic coordinate system is used. The contour plot by using Eq. (15) to represent $\frac{1}{2\pi} \ln r$ is shown in Fig. 2. The normal derivative along the boundary in the elliptic coordinates is defined by

$$\psi(x) = \frac{\partial \varphi(x)}{\partial n_x} = \frac{1}{J_x} \frac{\partial \varphi(x)}{\partial \xi}, \quad x \in B, \tag{16}$$

where J_x is the Jacobian term of a field point as shown below:

$$J_x = c\sqrt{(\sinh \xi \cos \eta)^2 + (\cosh \xi \sin \eta)^2}. \tag{17}$$

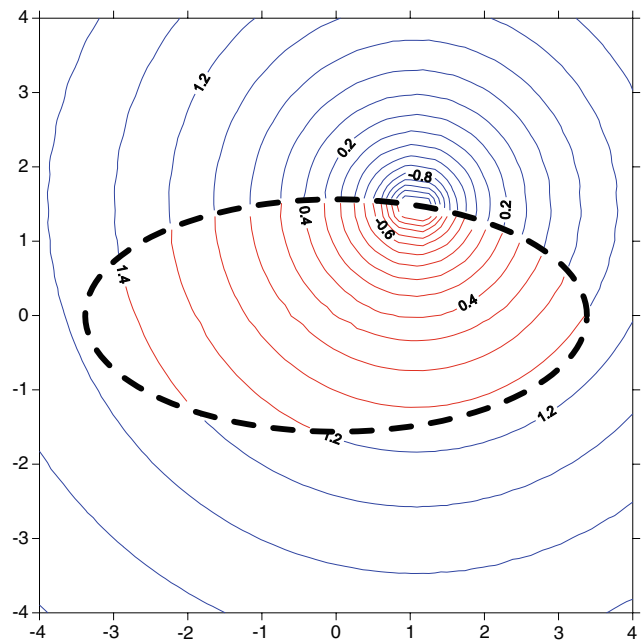


Fig. 2 Contour plot of the degenerate kernel in the elliptic coordinates

Then, $T(s, x)$ can be obtained as shown below by using Eq. (11)

$$T(s, x) = \begin{cases} T^i(\bar{\xi}, \bar{\eta}; \xi, \eta) = \frac{1}{J_s} \left(1 + 2 \sum_{m=1}^{\infty} e^{-m\bar{\xi}} \cosh m\xi \cos m\eta \cos m\bar{\eta} + 2 \sum_{m=1}^{\infty} e^{-m\bar{\xi}} \sinh m\xi \sin m\eta \sin m\bar{\eta} \right), & \bar{\xi} > \xi, \\ T^e(\bar{\xi}, \bar{\eta}; \xi, \eta) = \frac{1}{J_s} \left(-2 \sum_{m=1}^{\infty} e^{-m\xi} \sinh m\bar{\xi} \cos m\eta \cos m\bar{\eta} - 2 \sum_{m=1}^{\infty} e^{-m\xi} \cosh m\bar{\xi} \sin m\eta \sin m\bar{\eta} \right), & \bar{\xi} < \xi. \end{cases} \tag{18}$$

where J_s is the Jacobian term of a source point as shown below:

$$J_s = c\sqrt{(\sinh \bar{\xi} \cos \bar{\eta})^2 + (\cosh \bar{\xi} \sin \bar{\eta})^2}. \tag{19}$$

It can be noted that there is a Jacobian term in the denominator. The other kernels, $L(s, x)$ and $M(s, x)$, kernels can be easily derived by applying the derivative operators in

Eqs. (12) and (13) as shown below:

$$L(s, x) = \begin{cases} L^i(\bar{\xi}, \bar{\eta}; \xi, \eta) = \frac{1}{J_x} \left(-2 \sum_{m=1}^{\infty} e^{-m\bar{\xi}} \sinh m\xi \cos m\eta \cos m\bar{\eta} - 2 \sum_{m=1}^{\infty} e^{-m\bar{\xi}} \cosh m\xi \sin m\eta \sin m\bar{\eta} \right), & \bar{\xi} > \xi, \\ L^e(\bar{\xi}, \bar{\eta}; \xi, \eta) = \frac{1}{J_x} \left(1 + 2 \sum_{m=1}^{\infty} e^{-m\bar{\xi}} \cosh m\xi \cos m\eta \cos m\bar{\eta} + 2 \sum_{m=1}^{\infty} e^{-m\bar{\xi}} \sinh m\xi \sin m\eta \sin m\bar{\eta} \right), & \bar{\xi} < \xi, \end{cases} \quad (20)$$

$$M(s, x) = \begin{cases} M^i(\bar{\xi}, \bar{\eta}; \xi, \eta) = \frac{1}{J_s J_x} \left(2 \sum_{m=1}^{\infty} m e^{-m\bar{\xi}} \sinh m\xi \cos m\eta \cos m\bar{\eta} + 2 \sum_{m=1}^{\infty} m e^{-m\bar{\xi}} \cosh m\xi \sin m\eta \sin m\bar{\eta} \right), & \bar{\xi} \geq \xi, \\ M^e(\bar{\xi}, \bar{\eta}; \xi, \eta) = \frac{1}{J_s J_x} \left(2 \sum_{m=1}^{\infty} m e^{-m\bar{\xi}} \sinh m\xi \cos m\eta \cos m\bar{\eta} + 2 \sum_{m=1}^{\infty} m e^{-m\bar{\xi}} \cosh m\xi \sin m\eta \sin m\bar{\eta} \right), & \bar{\xi} < \xi. \end{cases} \quad (21)$$

For the boundary densities, we apply the Fourier expansions to approximate the potential, $\varphi(s)$, and its normal derivative, $\psi(s) = \frac{\partial u(s)}{\partial n_s} = \frac{1}{J_s} \frac{\partial \varphi(s)}{\partial \bar{\xi}}$, along the boundary as

$$\varphi(s) = a_0(\bar{\xi}) + \sum_{n=1}^{\infty} a_n(\bar{\xi}) \cos n\bar{\eta} + \sum_{n=1}^{\infty} b_n(\bar{\xi}) \sin n\bar{\eta}, \quad (\bar{\xi}, \bar{\eta}) \in B, \quad (22)$$

$$\psi(s) = \frac{1}{J_s(\bar{\xi}, \bar{\eta})} \left[a'_0(\bar{\xi}) + \sum_{n=1}^{\infty} a'_n(\bar{\xi}) \cos n\bar{\eta} + \sum_{n=1}^{\infty} b'_n(\bar{\xi}) \sin n\bar{\eta} \right], \quad (\bar{\xi}, \bar{\eta}) \in B, \quad (23)$$

respectively. It is noted that $\bar{\xi}$ is a constant along the elliptic boundary. Therefore, Eqs. (22) and (23) can be simplified to

$$\varphi(s) = a_0 + \sum_{n=1}^{\infty} a_n \cos n\bar{\eta} + \sum_{n=1}^{\infty} b_n \sin n\bar{\eta}, \quad (24)$$

$$\psi(s) = \frac{1}{J_s} \left(p_0 + \sum_{n=1}^{\infty} p_n \cos n\bar{\eta} + \sum_{n=1}^{\infty} q_n \sin n\bar{\eta} \right), \quad (25)$$

where a_0, a_n, b_n, p_0, p_n and q_n are the coefficients of the Fourier series, $\bar{\eta}$ is the angle ($0 \leq \bar{\eta} < 2\pi$). Here, it is observed that the term of J_s which may exist in the degenerate kernel, boundary density and boundary contour integral ($dB = Jd\bar{\eta}$) are cancelled out each other naturally in the boundary integral equation. Therefore, the elliptic integral is not required to deal with.

3.3 Adaptive observer system

After moving the point of Eq. (8) to the boundary, the boundary integrals through all the elliptic contours are required. Since the boundary integral equations are frame indifferent, *i.e.* objectivity rule is satisfied. The observer system is adaptive to locate the origin at the center of each ellipse in the boundary integrals. Adaptive observer system is chosen to fully employ the property of degenerate kernels. More detail can be found in [13–19]

3.4 Linear algebraic system

By moving the null-field point x_k to exactly locate on the k th elliptic boundary in the sense of limit for Eq. (8) in Fig. 1, we have

$$0 = \sum_{k=0}^N \int_{B_k} T(s, x) \varphi(s) dB_k(s) - \sum_{k=0}^N \int_{B_k} U(s, x) \psi(s) dB_k(s), \quad x \in D^c \cup B, \quad (26)$$

where $N + 1$ is the number of ellipses including the outer boundary and the inner elliptic inclusions. In the real computation, we select the collocation point on the boundary. It is noted that the integration path is counterclockwise for the outer ellipse. Otherwise, it is clockwise. For the integral of the elliptic boundary, the kernels of $U(s, x)$ and $T(s, x)$ are expressed in terms of degenerate kernels, and $\varphi(s)$ and $\psi(s)$ are substituted by using the Fourier series. In the B_k integral, we set the origin of the observer system to collocate at the center c_k to fully utilize the degenerate kernels and Fourier series. By collocating the null-field point exactly on the boundary, a linear algebraic system is obtained

$$[\mathbf{U}] \{\boldsymbol{\psi}\} = [\mathbf{T}] \{\boldsymbol{\varphi}\}, \quad (27)$$

where $[\mathbf{U}]$ and $[\mathbf{T}]$ are the influence matrices with a dimension of $(N + 1) \times (2L + 1)$ by $(N + 1) \times (2L + 1)$, $\{\boldsymbol{\varphi}\}$ and $\{\boldsymbol{\psi}\}$ denote the column vectors of Fourier coefficients with a dimension of $(N + 1) \times (2L + 1)$ by 1 in which $[\mathbf{U}]$, $[\mathbf{T}]$, $\{\boldsymbol{\varphi}\}$ and $\{\boldsymbol{\psi}\}$ can be defined as follows:

$$[\mathbf{U}_{ij}] = \begin{bmatrix} \mathbf{U}_{00} & \mathbf{U}_{01} & \cdots & \mathbf{U}_{0N} \\ \mathbf{U}_{10} & \mathbf{U}_{11} & \cdots & \mathbf{U}_{1N} \\ \vdots & \vdots & \ddots & \vdots \\ \mathbf{U}_{N0} & \mathbf{U}_{N0} & \cdots & \mathbf{U}_{NN} \end{bmatrix}, \quad (28)$$

$$[\mathbf{T}_{ij}] = \begin{bmatrix} \mathbf{T}_{00} & \mathbf{T}_{01} & \cdots & \mathbf{T}_{0N} \\ \mathbf{T}_{10} & \mathbf{T}_{11} & \cdots & \mathbf{T}_{1N} \\ \vdots & \vdots & \ddots & \vdots \\ \mathbf{T}_{N0} & \mathbf{T}_{N1} & \cdots & \mathbf{T}_{NN} \end{bmatrix}, \quad (29)$$

$$\{\varphi\} = \begin{Bmatrix} \varphi_0 \\ \varphi_1 \\ \varphi_2 \\ \vdots \\ \varphi_N \end{Bmatrix}, \tag{30}$$

$$\{\psi\} = \begin{Bmatrix} \psi_0 \\ \psi_1 \\ \psi_2 \\ \vdots \\ \psi_N \end{Bmatrix}, \tag{31}$$

where the vectors $\{\varphi_k\}$ and $\{\psi_k\}$ are in the form of $\{a_0^k, a_1^k, b_1^k \dots a_L^k, b_L^k\}^T$ and $\{p_0^k, p_1^k, q_1^k \dots p_L^k, q_L^k\}^T$, respectively; the first subscript “ j ” ($j = 0, 1, 2, \dots, N,$) in $[\mathbf{U}_{jk}]$ and $[\mathbf{T}_{jk}]$ denotes the index of the j th ellipse where the collocation point is located and the second subscript “ k ” ($k = 0, 1, 2, \dots, N,$) denotes the index of the k th ellipse where boundary data $\{\varphi_k\}$ and $\{\psi_k\}$ are specified and L indicates the truncated terms of Fourier series. The coefficient matrix of the linear algebraic system is partitioned into blocks, and each off-diagonal block corresponds to the influence matrices between two different elliptic inclusions. The diagonal blocks are the influence matrices due to itself in each individual hole. After uniformly collocating the null-field point along the k th elliptic boundary, the submatrix can be written as

$$[\mathbf{K}_{jk}] = \begin{bmatrix} K_{jk}^{0c}(\eta_1) & K_{jk}^{1c}(\eta_1) & K_{jk}^{1s}(\eta_1) & \dots & K_{jk}^{Lc}(\eta_1) & K_{jk}^{Ls}(\eta_1) \\ K_{jk}^{0c}(\eta_2) & K_{jk}^{1c}(\eta_2) & K_{jk}^{1s}(\eta_2) & \dots & K_{jk}^{Lc}(\eta_2) & K_{jk}^{Ls}(\eta_2) \\ K_{jk}^{0c}(\eta_3) & K_{jk}^{1c}(\eta_3) & K_{jk}^{1s}(\eta_3) & \dots & K_{jk}^{Lc}(\eta_3) & K_{jk}^{Ls}(\eta_3) \\ \vdots & \vdots & \vdots & \ddots & \vdots & \vdots \\ K_{jk}^{0c}(\eta_{2L}) & K_{jk}^{1c}(\eta_{2L}) & K_{jk}^{1s}(\eta_{2L}) & \dots & K_{jk}^{Lc}(\eta_{2L}) & K_{jk}^{Ls}(\eta_{2L}) \\ K_{jk}^{0c}(\eta_{2L+1}) & K_{jk}^{1c}(\eta_{2L+1}) & K_{jk}^{1s}(\eta_{2L+1}) & \dots & K_{jk}^{Lc}(\eta_{2L+1}) & K_{jk}^{Ls}(\eta_{2L+1}) \end{bmatrix}, \tag{32}$$

where K can be substituted by U or T . Although the matrix in Eq. (32) is not sparse, it is diagonally dominant. It is found that the influence coefficient for the higher-order harmonics is smaller. It is noted that the superscript “0s” in Eq. (32) disappears since $\sin(0\eta) = 0$. The element of $[\mathbf{K}_{jk}]$ is defined, respectively, as

$$K_{jk}^{nc}(\eta_m) = \int_{B_k} K(s_k, x_m) \cos(n\bar{\eta}_k) d\bar{\eta}_k, \tag{33}$$

$$K_{jk}^{ns}(\eta_m) = \int_{B_k} K(s_k, x_m) \sin(n\eta_k) \bar{\eta}_k d\bar{\eta}_k, \tag{34}$$

where $n = 0, 1, 2, \dots, L, m = 1, 2, \dots, 2L + 1$, and η_m is the angle coordinate of the elliptical coordinates of the collocating points x_m along the boundary. The physical meaning is that the influence coefficient of $U_{jk}^{nc}(\eta_m)$ in Eq. (34) denotes the response at x_m due to the $\cos(n\bar{\eta})$ dis-

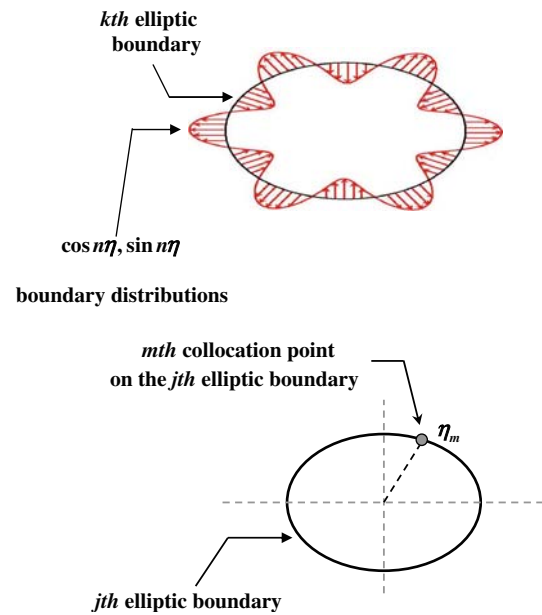


Fig. 3 Physical meaning of the influence coefficient $U_{jk}^{nc}(\eta_m)$

tribution as shown in Fig. 3. By rearranging the known and unknown sets, the unknown Fourier coefficients are determined. Equation (8) can be calculated by employing the orthogonal relations of trigonometric functions in the real computation. Only the finite L terms are used in the summation of Eqs. (24) and (25).

By using the concept of domain decomposition, the problem in Fig. 1 can be decomposed into two parts as shown in Fig. 4a, b. One is the torsion problem of a elliptic bar with two elliptic holes and the other is a problem of each inclusion. For the torsion problem with elliptic holes which satisfies the Laplace equation, the linear algebraic system from Eq. (27) can be obtained as

$$\begin{bmatrix} \mathbf{T}_{00}^M & \mathbf{T}_{01}^M & \dots & \mathbf{T}_{0N}^M & -\mathbf{U}_{01}^M & \dots & -\mathbf{U}_{0N}^M \\ \mathbf{T}_{10}^M & \mathbf{T}_{11}^M & \dots & \mathbf{T}_{1N}^M & -\mathbf{U}_{11}^M & \dots & -\mathbf{U}_{1N}^M \\ \vdots & \vdots & \ddots & \vdots & \vdots & \ddots & \vdots \\ \mathbf{T}_{N0}^M & \mathbf{T}_{N1}^M & \dots & \mathbf{T}_{NN}^M & -\mathbf{U}_{N1}^M & \dots & -\mathbf{U}_{NN}^M \end{bmatrix} \times \begin{Bmatrix} \varphi_0^M \\ \varphi_1^M \\ \vdots \\ \varphi_N^M \\ \psi_1^M \\ \vdots \\ \psi_N^M \end{Bmatrix} = \begin{Bmatrix} \mathbf{0} \\ \mathbf{0} \\ \vdots \\ \mathbf{0} \end{Bmatrix}. \tag{35}$$

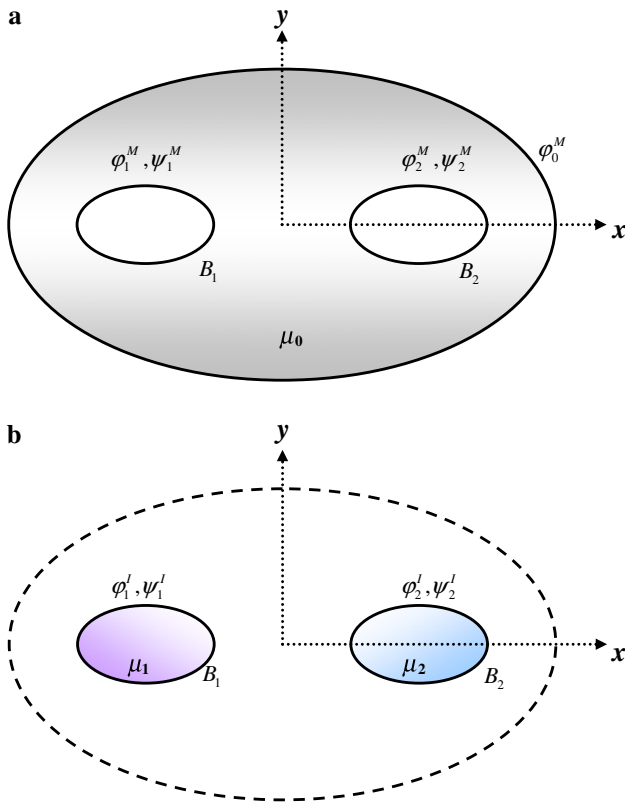


Fig. 4 a Torsion problem of an elliptic bar with elliptic holes. b Each elliptic inclusion problem

For each inclusion, we have

$$\begin{bmatrix} \mathbf{T}_{11}^I & \mathbf{0} & \mathbf{0} & -\mathbf{U}_{11}^I & \mathbf{0} & \mathbf{0} \\ \mathbf{0} & \ddots & \mathbf{0} & \mathbf{0} & \ddots & \mathbf{0} \\ \mathbf{0} & \mathbf{0} & \mathbf{T}_{NN}^I & \mathbf{0} & \mathbf{0} & -\mathbf{U}_{NN}^I \end{bmatrix} \begin{bmatrix} \varphi_1^I \\ \vdots \\ \varphi_N^I \\ \psi_1^I \\ \vdots \\ \psi_N^I \end{bmatrix} = \begin{bmatrix} \mathbf{0} \\ \vdots \\ \mathbf{0} \end{bmatrix}. \tag{36}$$

In order to satisfy the continuity conditions of displacement and equilibrium condition of traction on the interface, we have

$$\{\varphi_i^M\} - \{\varphi_i^I\} = \{\mathbf{0}\}, \tag{37}$$

$$\mu_0 \{\psi_i^M\} - \mu_i \{\psi_i^I\} = \{\mathbf{b}_i\}, \tag{38}$$

where $\{\mathbf{b}_i\}$ is

$$\{\mathbf{b}_i\} = \begin{bmatrix} (\mu_0 - \mu_i)(e_y^i n_{x1}^i - e_x^i n_{y1}^i) \\ (\mu_0 - \mu_i)(e_y^i n_{x2}^i - e_x^i n_{y2}^i) \\ \vdots \\ (\mu_0 - \mu_i)(e_y^i n_{x2M}^i - e_x^i n_{y2M}^i) \\ (\mu_0 - \mu_i)(e_y^i n_{x2M+1}^i - e_x^i n_{y2M+1}^i) \end{bmatrix}, \tag{39}$$

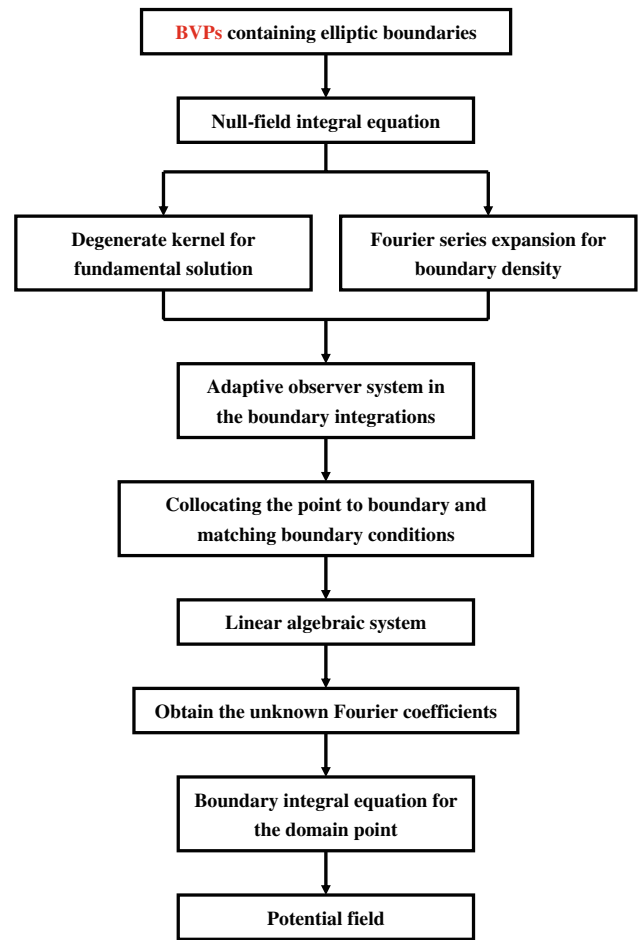


Fig. 5 Flowchart of the present approach

where

$$n_{x_j}^i = \frac{\sinh \xi_i \cos \eta_j}{\sqrt{(\sinh \xi_i \cos \eta_j)^2 + (\cosh \xi_i \sin \eta_j)^2}}, \tag{40}$$

$$n_{y_j}^i = \frac{\cosh \xi_i \sin \eta_j}{\sqrt{(\sinh \xi_i \cos \eta_j)^2 + (\cosh \xi_i \sin \eta_j)^2}}. \tag{41}$$

Combining with the above mentioned linear algebraic system of Eqs. (35)–(38), the global linear algebraic equation can be obtained by correctly arranging the Fourier coefficients. After obtaining the Fourier coefficients, the torsional rigidity, G , can be easily determined as follows:

$$G = \mu \int_D (x^2 + y^2) dD - \mu \sum_{k=1}^N \int_{B_k} \varphi \frac{\partial \varphi}{\partial n} dB_k, \tag{42}$$

$$G^T = G^M + G^I, \tag{43}$$

where the subscripts of “ T ”, “ M ” and “ I ” denote the torsion rigidity of total, matrix and inclusion, respectively. For clarity, the flowchart of our method is shown in Fig. 5.

Table 2 Dimensionless torsional rigidity and maximum shear stresses of the composite elliptic bar

μ_1/μ_0	μ_2/μ_0	Torsional rigidity \bar{G}				$\bar{\tau}_{\max}$			
		Katsikadelis and Sapountzakis	Chou and Shamas-Ahmadi	Sapountzakis and Mokos	Present	Katsikadelis and Sapountzakis	Chou and Shamas-Ahmadi	Sapountzakis and Mokos	Present
0.0	0.0	0.2934	0.2842	0.2857	0.2857	0.8142	0.7883	0.7922	0.7901
	0.4	0.2968	0.2921	0.2948	0.2948	0.8091	0.7820	0.8042	0.8068
	1.0	0.3047	0.2971	0.2992	0.2992	0.8072	0.7869	0.8116	0.8139
0.2	0.2	0.2974	0.2954	0.2980	0.2980	0.8108	0.7895	0.7596	0.7594
	0.6	0.2980	0.3000	0.3033	0.3033	0.8054	0.7821	0.7738	0.7731
	1.0	0.3029	0.3030	0.3058	0.3059	0.8038	0.7811	0.7802	0.7790
0.4	0.4	0.3001	0.3008	0.3046	0.3046	0.8036	0.7737	0.7770	0.7768
	0.6	0.3024	0.3028	0.3067	0.3067	0.8027	0.7790	0.7824	0.7821
	1.0	0.3076	0.3060	0.3093	0.3093	0.8016	0.7875	0.7887	0.7882
0.6	0.6	0.3048	0.3048	0.3088	0.3088	0.8017	0.7839	0.7876	0.7875
	0.8	0.3037	0.3065	0.3103	0.3103	0.8010	0.7884	0.7914	0.7911
	1.0	0.3099	0.3081	0.3114	0.3115	0.8006	0.7924	0.7940	0.7937
0.8	0.8	0.3098	0.3082	0.3118	0.3118	0.8004	0.7925	0.7949	0.7948
	1.0	0.3124	0.3098	0.3130	0.3130	0.8000	0.7965	0.7976	0.7974
1.0	1.0	0.3150	0.3114	0.3141	0.3142	0.7989	0.8003	0.8001	0.8000

4 An illustrative example and discussions

An elliptic bar with two symmetrical elliptic inclusions is considered here. The sketch of cross section is depicted in Fig. 1. In Table 2, the dimensionless torsional rigidity and maximum shear stresses are defined as $\bar{G} = G/\mu_0 L^4$ and $\bar{\tau}_{\max} = \tau_{\max}/\mu_0 \alpha L$ versus various values of ratios μ_1/μ_0 and μ_2/μ_0 . The data of Katsikadelis and Sapountzakis [5], Shams-Ahmadi and Chou [8], and Sapountzakis and Mokos [9] are used to compare with our results. In the numerical implementation of the present approach, the number of Fourier series is 41 and 41 nodes are uniformly distributed in the η coordinate on each boundary. As shown in Table 2, the torsional rigidities of present approach match well with those of Sapountzakis and Mokos [9], but they deviate among the results of Katsikadelis and Sapountzakis [5], Shams-Ahmadi and Chou [8] and ours. The data are the results of torsional rigidity. Their error is also larger than ours. For the maximum shear stress ($\bar{\tau}_{\max}$), our data are close to those of the Sapountzakis and Mokos' results and the relative error is less than 1%. However, it is observed that the results of Katsikadelis and Sapountzakis are greater than others. Maybe, more number of boundary elements is required. In this example, high accuracy of the present approach is obtained not only for torsion rigidity but also shear stress.

5 Conclusions

We have successfully proposed a systematic method by using the null-field integral formulation in conjunction with degen-

erate kernels and Fourier series for solving the torsion problems of an elliptic composite bar. The fundamental solution was expanded to a degenerate kernel by using the elliptic coordinates in this paper. Although a Jacobian term may appear in the degenerate kernel, boundary density and boundary contour integral by using the elliptic coordinates, it can be cancelled out in the BIE. Free of calculating principal value of using bump contour method is our advantage than the conventional boundary integral equation thanks to the degenerate kernel. Besides, stress and torsional rigidity were both obtained by using the proposed approach. Our results matched well with those of the complex-variable method and BEM. Although only an example of an elliptic bar with two elliptic inclusions was given to show the validity of our approach, the more general case with the arbitrary number, different size and various position of elliptic inclusion can be solved by using the developed program.

Acknowledgments Financial support from the National Science Council under Grant No. NSC-98-2221-E019-007-Mr3 is gratefully acknowledged.

References

1. Chou PC, Pagano J (1992) Elasticity: tensor, dyadic, and engineering approaches. Dover, New York
2. Reismann H, Pawlik PS (1980) Elasticity: theory and applications. Wiley, New York
3. Timoshenko SP, Goodier JN (1970) Theory of elasticity. McGraw-Hill, New York

4. Yao W, Zhong W, Lim CW (2009) Symplectic elasticity. World Scientific Publishing, Singapore
5. Katsikadelis JT, Sapountzakis EJ (1985) Torsion of composite bars by boundary element method. *ASCE J Eng Mech* 111:1197–1210
6. Chou SI, Shams-Ahmadi M (1992) Complex variable boundary element method for torsion of hollow shafts. *Nuclear Eng Des* 136:255–263
7. Hromadka TV, Lai C (1986) The complex variable boundary element method in engineering analysis. Springer, New York
8. Shams-Ahmadi M, Chou SI (1997) Complex variable boundary element method for torsion of composite shafts. *Int J Numer Methods Eng* 40:1165–1179
9. Sapountzakis EJ, Mokos VG (2001) Nonuniform torsion of composite bars by boundary element method. *ASCE J Eng Mech* 127(9):945–953
10. Sapountzakis EJ, Mokos VG (2003) Warping shear stresses in non-uniform torsion of composite bars by BEM. *Comput Methods Appl Mech Eng* 192:4337–4353
11. Sapountzakis EJ, Mokos VG (2004) Nonuniform torsion of composite bars of variable thickness by BEM. *Int J Solids Struct* 41(7):1753–1771
12. Chen JT, Hsiao CC, Leu SY (2006) Null-field integral equation approach for plate problems with circular boundaries. *ASME J Appl Mech* 73:679–693
13. Chen JT, Shen WC, Chen PY (2006) Analysis of circular torsion bar with circular holes using null-field approach. *CMES* 12: 109–119
14. Chen JT, Shen WC, Wu AC (2006) Null-field integral equations for stress field around circular holes under anti-plane shear. *Eng Anal Bound Elem* 30(3):205–217
15. Chen JT, Wu AC (2006) Null-field approach for piezoelectricity problems with arbitrary circular inclusions. *Eng Anal Bound Elem* 30:971–993
16. Chen JT, Chen CT, Chen PY, Chen IL (2007) A semi-analytical approach for radiation and scattering problems with circular boundaries. *Comput Methods Appl Mech Eng* 196:2751–2764
17. Chen JT, Lee YT, Chou KS (2010) Revisit of two classical elasticity problems by using the null-field integral equations. *J Mech* (accepted)
18. Chen JT, Lee YT, Lin YJ (2009) Interaction of water waves with arbitrary vertical cylinders using null-field integral equations. *Appl Ocean Res* 31(2):101–110
19. Chen JT, Lee YT (2009) Torsional rigidity of a circular bar with multiple circular inclusions using the null-field integral approach. *Comput Mech* 44(2):221–232
20. Chen JT, Wu AC (2007) Null-field approach for the multi-inclusion problem under anti-plane shears. *ASME J Appl Mech* 74:469–487
21. Chen JT, Hsiao CC, Leu SY (2008) A new method for Stokes' flow with circular boundaries using degenerate kernel and Fourier series. *Int J Numer Methods Eng* 74:1955–1987
22. Chen JT, Ke JN (2008) Derivation of anti-plane dynamic Green's function for several circular inclusions with imperfect interfaces. *CMES* 29(3):111–135
23. Atkinson KE (1997) The numerical solution of integral equations of the second kind. Cambridge University Press, New York
24. Golberg MA (1979) Solution methods for integral equations: theory and applications. Plenum Press, New York
25. Porter D, Stirling DSG (1990) Integral equations: a practical treatment, from spectral theory to applications. Cambridge University Press, New York
26. Sloan IH, Burn BJ, Datyner N (1975) A new approach to the numerical solution of integral equations. *J Comput Phys* 18: 92–105
27. Kress R (1989) Linear integral equation. Springer, New York
28. Kress R (1995) On the numerical solution of a hypersingular integral equation in scattering theory. *J Comput Appl Math* 61: 345–360
29. Morse PM, Feshbach H (1978) Methods of theoretical physics. McGraw-Hill, New York